Measurement of Low-Q^2 Protons from Neutral Current Events in Argon with MicroBooNE

MICROBOONE-NOTE-1067-PUB

The MicroBooNE Collaboration*

June 17, 2020

Abstract

The MicroBooNE experiment is an 85 ton active mass liquid-argon time projection chamber located at the Fermilab Booster Neutrino Beamline. MicroBooNE's ability to detect low-energy protons allows us to study single-proton events with a four-momentum transfer squared Q^2 as low as 0.10 GeV^2. We present a differential cross-section measurement of a signal with one proton and no other particles (NC1p) in the final state. We report the flux-averaged NC1p differential cross section $d\sigma/dT$ for neutrinos scattering on argon as a function of proton kinetic energy T using a subset of MicroBooNE's data.

*Email: MICROBOONE_INFO@fnal.gov

Contents

1 Introduction

Better knowledge of both charged-current (CC) and neutral-current (NC) neutrino-nucleus interactions is essential for interpreting the data of future long-baseline neutrino oscillation experiments, such as Deep Underground Neutrino Experiment (DUNE) [1]. It is also a useful tool to study the nucleon and nuclear structure. NC interactions are considered an important tool in the search for sterile neutrinos through beam disappearance [2], as all active neutrino species participate, unlike in the CC case. Currently, there is very little data of cross sections for NC interactions with argon.

The NC interaction occurs through the exchange of a Z^0 boson. Other than the invisible neutrino that remains the same flavor after the interaction, the final state particle(s) being detected could be the nucleon that the neutrino knocked out from the nucleus, or other particles that are produced at the interaction vertex or after final state interaction (FSI) and secondary re-interaction outside the nucleus. Studying NC interactions is very useful to determine the hadronic weak current. In particular, neutral-current elastic scattering, in which the neutrino elastically scatters from a proton, is a useful tool to determine the strange quark contribution to the spin structure of the nucleon [3].

The probability of an NC interaction occurring is less than 50% smaller than for a CC interaction and with only hadrons in the final state it is more difficult to measure the NC interactions. We present here the first inclusive cross section measurement in argon of NC events with one proton in the final state (NC1p). In addition to being an interesting measurement in its own right, this represents an important milestone towards measuring the NC Elastic (NCE) cross section and determining the strange quark contribution to the spin of the nucleon.

2 MicroBooNE Experiment

The MicroBooNE [4] experiment is an 85 ton active mass liquid-argon time projection chamber (LArTPC) located at the Fermilab Booster Neutrino Beamline (BNB). The BNB is a predominantly ν_μ beam with peak energy around 700 MeV. MicroBooNE's active region is $2.3 \times 2.5 \times 10.4$ m^3. Figure 1 shows a schematic of the MicroBooNE TPC [5]. Charged particles produced from neutrino interactions ionize the argon along their path. The ionization electrons drift in a 273 V/cm electric field along the x axis, towards the vertical (y, z) anode plane for readout. The fiducial volume of the detector is defined as the region 10 cm from the edges of the TPC in x and z directions and, 20 cm from the edge in y direction.

In addition to the wire chamber, the experiment employs a set of 32 8-inch cryogenic photomultiplier tubes (PMTs) located directly behind the anode plane, in order to take advantage of the excellent scintillation properties of argon that it produces a large amount of light per unit energy deposited (about 24,000 photons per MeV at 500 V/cm drift field) and is transparent to its own scintillation. Light detected by the PMTs is used as a trigger for the presence of interesting neutrino interactions, as well as for rejecting cosmic-ray events. This trigger looks at light activity on the PMTs in time-coincidence with the 1.6 μs beam-spill reaching the detector, which may be caused by a neutrino interaction or coincident cosmic activity.

MicroBooNE has been taking neutrino-beam data since October 2015, and has collected a total of 1.56×10^{21} protons on target (POT). In this note, we present a result using a subset (0.5×10^{21} POT) of data. Two different data streams are used in this analysis. The on-beam data stream ("BNB") is triggered by BNB neutrino spills that last for 1.6 μs. The off-beam data stream ("EXT") is taken during periods when no beam was received but is triggered by coincident cosmic activity. The off-beam data sample is used to measure the cosmic-ray backgrounds, which are appreciable due to the location of MicroBooNE near the surface and without substantial overhead shielding.

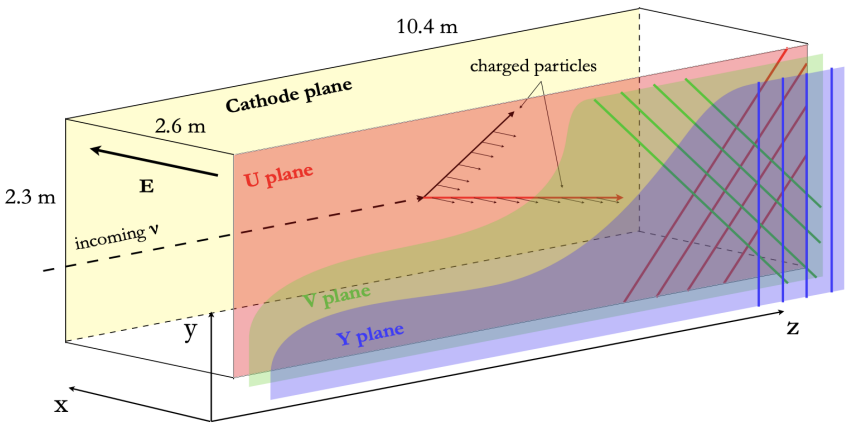

Figure 1: A schematic of the MicroBooNE TPC system from [5].

3 Signal and Background Definitions

NC1p stands for a signal of only one proton above some threshold and no other particles above threshold in the final state. Due to the poor reconstruction efficiency at very low momenta, the momentum threshold for protons is 200 MeV/c, for muons 100 MeV/c, and for pions 65 MeV/c; there is no requirement on neutrons, which are not detected (*i.e.* there could be any number of neutrons). NC1p includes all following categories as long as they satisfy the one proton requirement.

1. Neutral-current elastic (NCE) scattering off a proton.
2. Neutral-current elastic scattering off a neutron that re-interacts in the nucleus and knocks out a proton.
3. Neutral-current meson exchange current (MEC) events with one proton in the final state.
4. Neutral-current resonance (RES) or deep inelastic interactions (DIS) with one proton and no other particles above threshold in the final state.

The signal events are defined to be from ν_μ only, and labeled as "$\nu_\mu\, 0\mu 0\pi 1p$ Proton" in the plots of this note. The main sources of our background are

1. Protons from CC events, where the muon was not detected. These events are labeled as "CC Proton" in the plots of this note.
2. Reconstructed events coming from a cosmic-induced interaction that triggered the readout of the detector. These are modeled using random triggers with coincident cosmic activity during a false beam-window. These events are labeled as "Cosmics (Data)" in the plots of this note.
3. NC proton events that have more than 1 proton in the final state, or have both proton(s) and pion(s) in the final state. These events are labeled as "NC Proton + X" in the plots of this note.
4. Events in which the selected track is a cosmic track from a readout triggered by a neutrino interaction. These events are labeled as "Cosmics (Overlay)" in the plots of this note.
5. Events in which the selected track is not a proton. These events are labeled as "Non-Proton" in the plots of this note.
6. Single-proton events that satisfy the signal definition, but are outside of the fiducial volume. These events are labeled as "OutFV" in the plots of this note.
7. Single-proton events that satisfy the signal definition, but are generated from $\bar{\nu}_\mu$ and ν_e events. These events are labeled as "$\bar{\nu}_\mu\, 0\mu 0\pi 1p$" and "$\nu_e\, 0\mu 0\pi 1p$ Proton" in the plots of this note.

In Section 6 the second class of backgrounds "Cosmics (Data)" is referred to as B_i^{EXT}, and all other backgrounds are summed together and referred to as B_i^{MC}.

4 Neutrino Interaction Simulation

In MicroBooNE, we use a cosmic-data-overlaid Monte Carlo (MC) sample to develop the analysis. The neutrino interactions are generated using the GENIE neutrino event generator version 3.0.4 [6, 7]. We apply extra corrections to obtain a GENIE 3.0.6 "MicroBooNE tune" [8] as our central value cross section models.

The NC models being used in the generator are summarized in Table 1. Details on all models used in GENIE and their associated uncertainties can be found in Ref. [8].

Model	Parameter	Description
Nuclear model	LFG	Local Fermi Gas model
Final State Interaction Model	hA2018	Hadron-nucleus interaction model
NC Elastic model	$M_A = 0.96$ GeV	Axial mass in Ahrens model
	$\eta = 0.12$	Strange quark contribution in Ahrens model
NC Resonance model	$M_A = 1.120$ GeV	Axial mass of Berger-Sehgal model
	$M_V = 0.840$ GeV	Vector mass of Berger-Sehgal model
NC Meson Exchange Current model	-	Empirical Dytman model

Table 1: List of models that are being used in GENIE 3.0.6 for generating neutral-current events.

5 Event Reconstruction and Selection

MicroBooNE employs signal processing [9, 10] to convert 2D raw-data into Gaussian-shaped signals (known as "hits"). We then employ the Pandora multi-algorithm pattern recognition framework [11] to convert these 2D hits into 3D objects and create "Particle Flow Particles" ("PFParticles"), each of which corresponds to a track or shower, and their parent-daughter relationships between tracks and showers.

5.1 Proton Energy Reconstruction

The kinetic energy T of a candidate proton track is calculated from its track length L, using

$$T = a \cdot L^b, \tag{1}$$

in which $a = 31.3$, $b = 0.578$ are determined by fitting to the PSTAR [12] data. For protons that have kinetic energy $50 < T < 500$ MeV, their length is $2.3 < L < 115.7$ cm, according to this parameterisation.

The reconstructed four-momentum transfer is taken as $Q^2 = 2TM$ [3], which is exact for elastic scattering from a free proton initially at rest, with M the proton mass and T the kinetic energy. Therefore, for an event with a 50 MeV proton in the final state, the four-momentum transfer is roughly 0.1 GeV^2.

5.2 Single Proton Event Selection

We require tracks to be contained within the fiducial volume and have a length $1.2 < L < 200$ cm. We remove events that have more than one object in the particle-flow hierarchy, as reconstructed by Pandora, and obvious cosmic backgrounds based on the light information [13]. We only keep track candidates that are going forward along the beam direction ($\cos\theta > 0$), since the low-energy protons we are interested in tend to be forward-going. To enrich our sample in protons we only select tracks that have a deposited energy profile consistent with a proton [14].

To further reduce the cosmic background, we created a multi-class gradient-boosted decision tree (BDT) classifier using the TMVA [15] package in ROOT. The variables used for the training include the total and track-end dE/dx on the collection plane, track start and end positions in cartesian coordinates, PID variables on all planes, track angles, and track length. Detailed descriptions of those variables are listed in Table 2.

Name in Figure 2	Description
EnddEdx	Sum of dE/dx for the last 6 hits of a candidate track
Phi	The angle between the candidate track direction and a horizontal line pointing away from the anode
TrkDist	The ratio of distance to the closest neighboring track/length
chi2-p-2	Proton PID variable on Plane Y
chi2-p-1	Proton PID variable on Plane V
Theta	The angle between the neutrino beam and the candidate track
EndY	The end position of the candidate track in Y
chi2-p-0	Proton PID variable on Plane U
Length	Length of the candidate track
StartY	The start position of the candidate track in Y
StartZ	The start position of the candidate track in Z
TotaldEdx	Sum of dE/dx of all hits of a candidate track
EndZ	The end position of the candidate track in Z

Table 2: Description of variables in the BDT training.

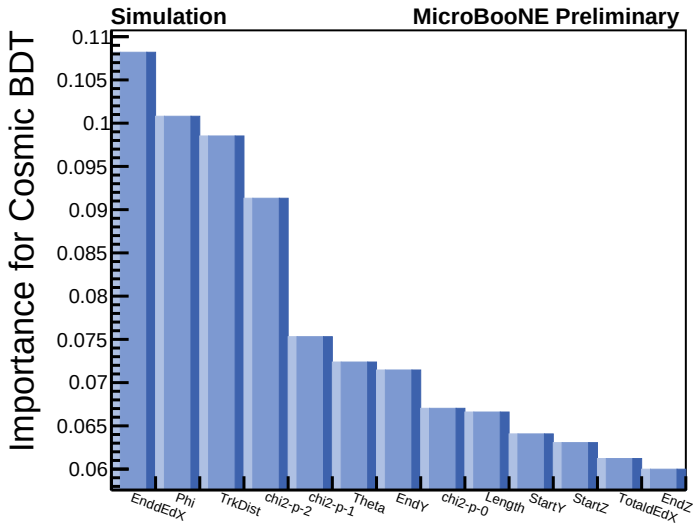

Figure 2: Importance of variables for cosmic BDT. Detailed descriptions are in Table 2.

The importance of each variable in the BDT is shown in Figure 2, it is derived by counting how often the variables are used to split decision tree nodes.

Figure 3 shows the data-to-MC comparison of the BDT response for the candidate NC1p events. We select events with BDT response above 0.2, which removes about 65% cosmic background and 10% signal events.

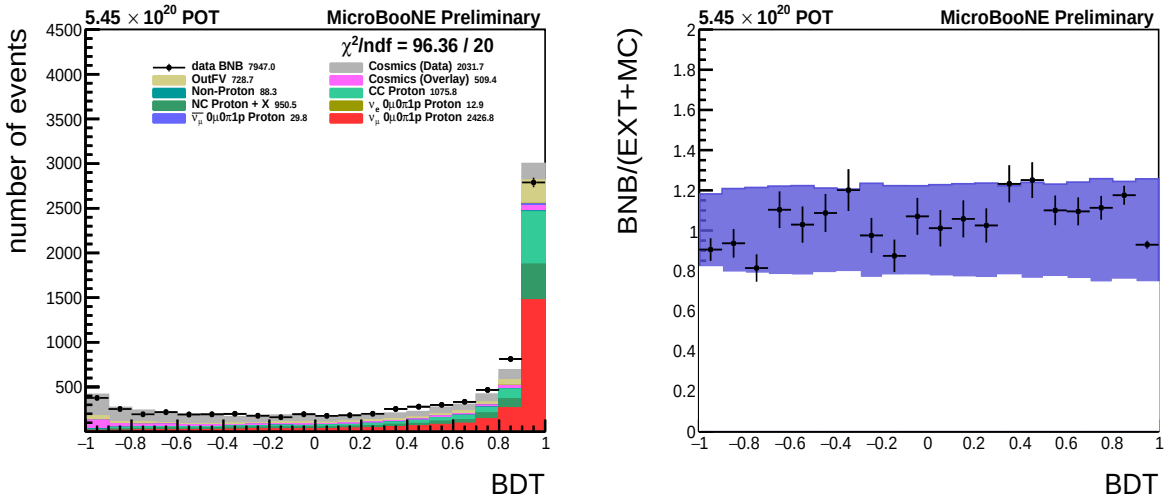

Figure 3: BDT response (left) of the candidate NC1p events. The right plot shows the ratio of beam-on data to the prediction of the BDT response. The purple band displays the systematic uncertainty that comes from the cross-section model, flux and secondary interaction.

Figure 4 shows the reconstructed kinetic energy T of candidate NC1p events, after the application of the BDT cut. The left plot shows the data-to-MC comparison and the right plot shows the ratio with full systematics, as described in Sec. 6. Figure 5 shows the track start positions of the selected events.

The selection efficiency as a function of true kinetic energy T before and after we apply the BDT cut is shown in the left plot of Figure 6, and the selection purity as a function of reconstructed kinetic energy is shown it the right plot of Figure 6. The overall selection efficiency is 29.8% for the energy region $0.05 < T < 0.5$ GeV, while the overall purity in the same energy region is 42.1%.

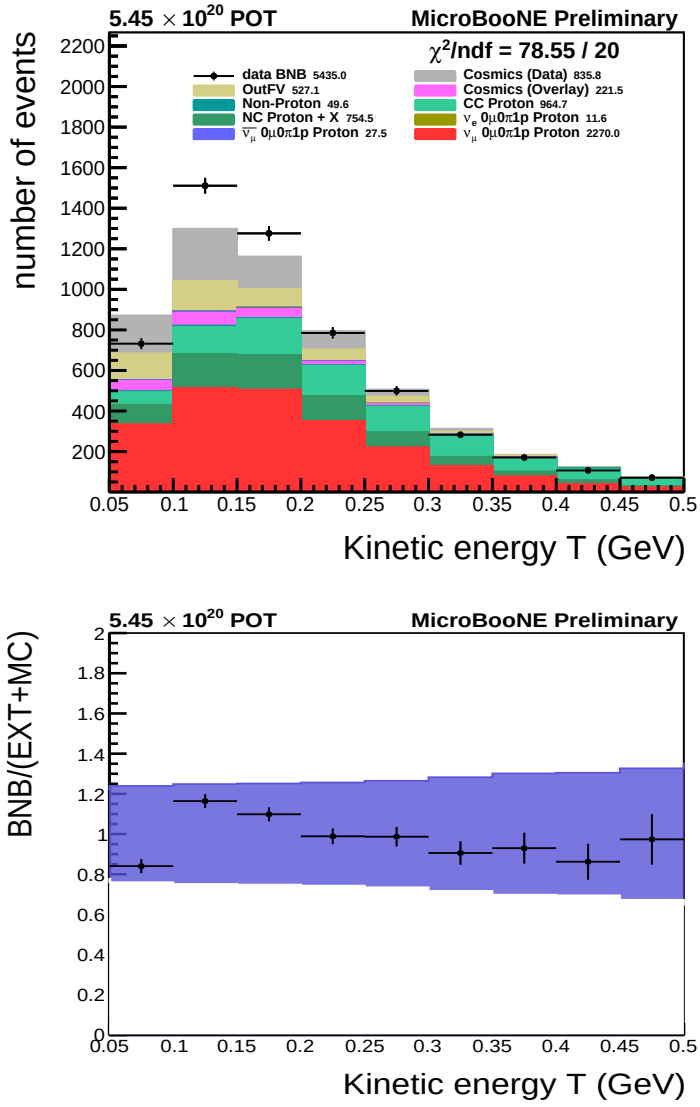

Figure 4: Reconstructed kinetic energy T of the candidate NC1p events. The stacked histograms in the top plot are broken down to highlight the signals and backgrounds. The bottom plot shows the ratio of BNB/(EXT+MC), which is the ratio of beam-on data to the prediction. The purple band shows the systematic uncertainty coming from the cross-section model, flux and secondary interaction.

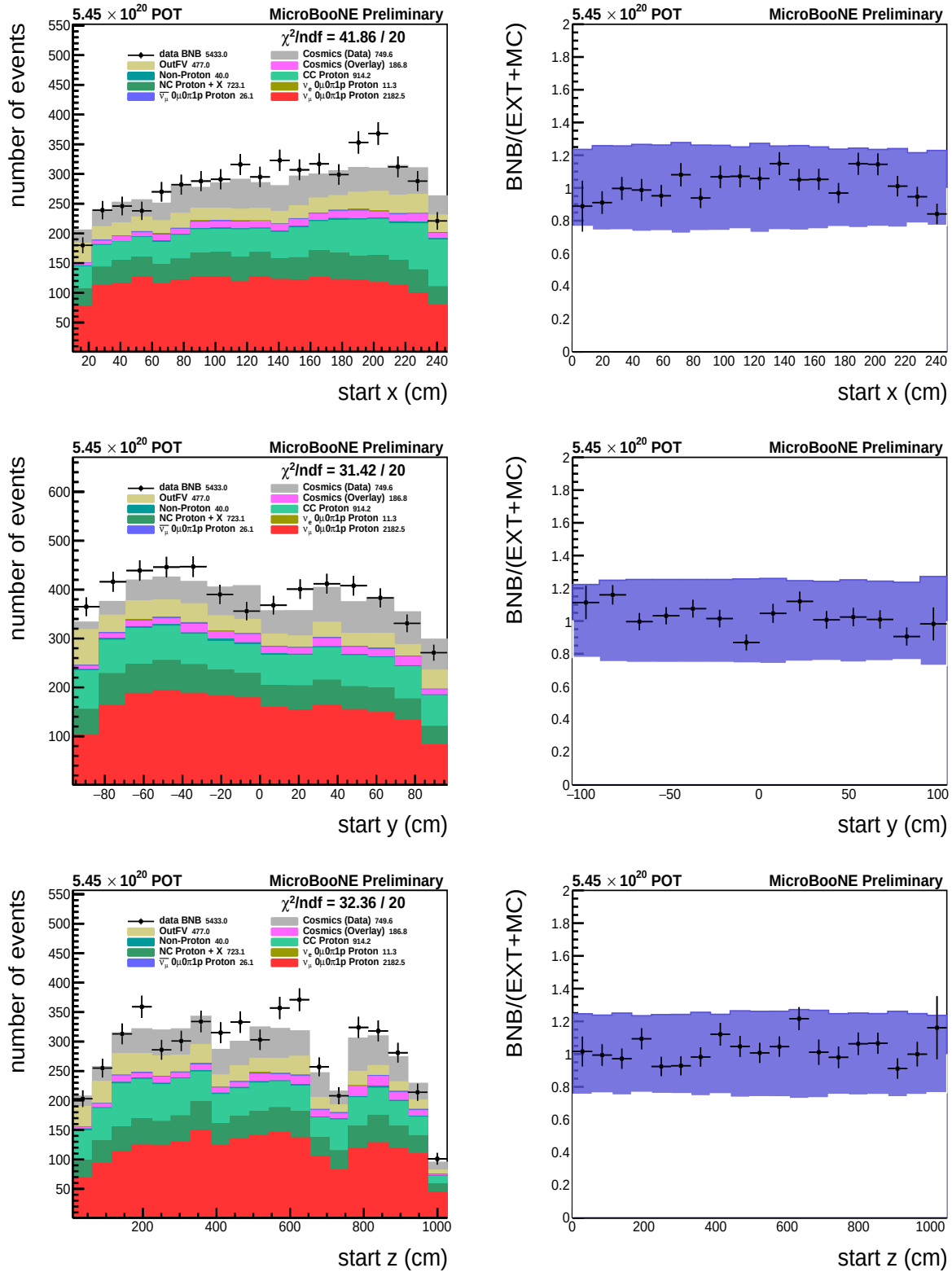

Figure 5: Track start x, y, and z distributions of the selected events. The stacked histograms in the top left plot are broken down to highlight the signals and backgrounds. The right plot shows the ratio of BNB/(EXT+MC), which is the ratio of beam-on data to the prediction. The purple band shows the total uncertainty coming from the cross-section model, flux and secondary interaction.

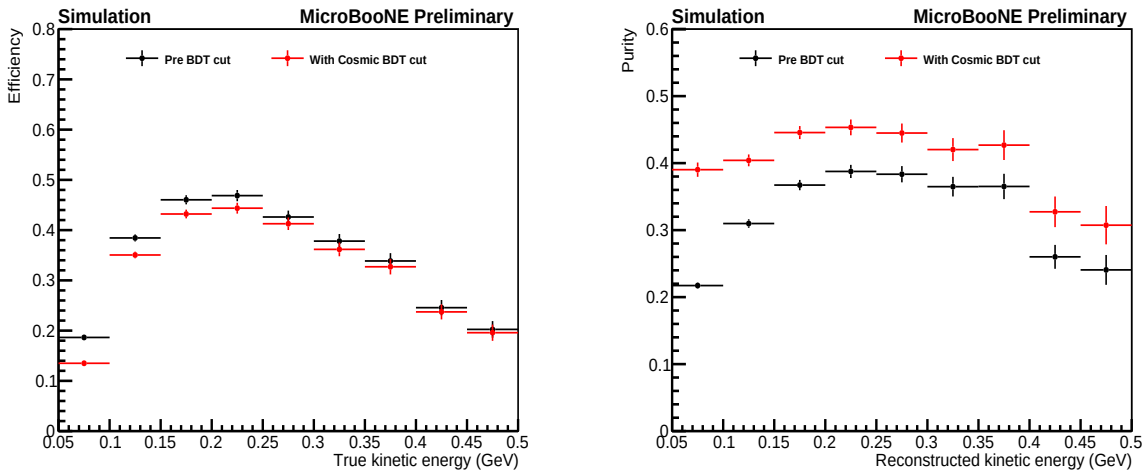

Figure 6: Selection efficiency (left) and purity (right) before and after applying the BDT cut, vs. kinetic energy T. The efficiency is shown as a function of true T and the purity is shown as a function of reconstructed T.

6 Differential Cross Section Extraction

In this section, we present the differential cross section $d\sigma/dT$ using a forward-folding method [16] in the energy range $0.05 < T < 0.5$ GeV.

The differential cross section can be written as

$$\left(\frac{d\sigma}{dT}\right)_i = \frac{N_i - B_i}{\epsilon_i \cdot N_{\text{target}} \cdot \Phi_{\nu_\mu} \cdot (\Delta T)_i} \tag{2}$$

where i is the i-th reconstructed T bin, N_i is the event count in bin i, $B_i = B_i^{\text{EXT}} + B_i^{\text{MC}}$ is the background in bin i; ϵ_i is the efficiency in bin i, defined as

$$\epsilon_i = \frac{\Sigma_{j=1}^{M} S_{ij} N_j^{\text{selected}}}{\Sigma_{j=1}^{M} S_{ij} N_j^{\text{generated}}} \tag{3}$$

where j is the j-th true T bin, N_j^{selected} is the number of selected true signal events and $N_j^{\text{generated}}$ are the generated signal events in the same bin.

The smearing matrix S_{ij}, as shown in Figure 7 (right), giving the probability that an event in a certain reconstructed bin originated in the same true bin, is defined as

$$S_{ij} = \frac{M_{ij}}{\Sigma_k M_{ik}} \tag{4}$$

in which M_{ij} is the i-th reconstructed and j-th truth bin of the migration matrix as shown in Figure 7 (left).

Note that both underflow ($0 < T < 0.05$ GeV) and overflow ($0.5 < T < 0.55$ GeV) bins are shown in Figure 7. We will not include those bins in the differential cross section result.

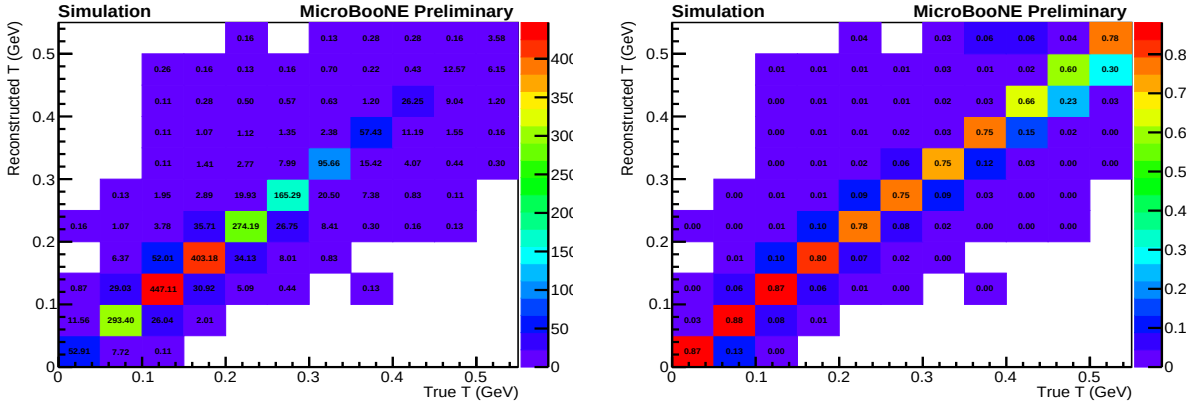

Figure 7: Left: the migration matrix for selected signal events. Right: The smearing function S_{ij} that is used to obtain the efficiency correction.

Figure 8 shows the smeared efficiency correction in reconstructed T, as defined in Eq. 3.

The number of target protons N_{target} is calculated to be 1.73856×10^8. The integrated flux is $\Phi_{\nu_\mu} = 4.00 \times 10^{11}/\text{cm}^2$. The kinetic-energy bin size is $\Delta T_i = 0.05$ GeV for all the bins.

The statistical uncertainty of the differential cross section is propagated from the event rate N_i, the background B_i, and the efficiency correction ϵ_i.

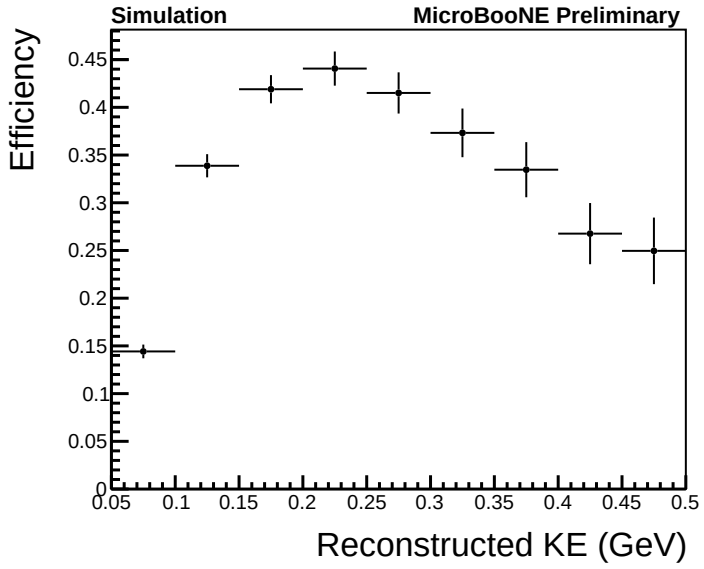

Figure 8: Smeared efficiency correction in reconstructed T.

7 Systematic Uncertainties

The systematic uncertainties considered come from the underlying neutrino interaction model, modeling of secondary hadronic re-interactions, modeling of the neutrino flux, uncertainties related to the electron drift/light propagation model and detector response.

The systematic uncertainties on the differential cross section are evaluated by re-extracting the differential cross section with varied background, efficiency correction and integrated flux terms.

For the cross section model, secondary re-interaction model and flux uncertainties, we use the "multisim" technique, which consists of generating several MC samples, each one called a "universe" with parameters in the models varied within their uncertainties, also taking into account correlations [8]. We re-extract the cross section σ^s from each universe s. The mean of the cross sections from the $N_s = 1000$ (500 for cross section model uncertainty) universes is defined as

$$m_i = \frac{1}{N_s}\Sigma_s \sigma_i^s. \tag{5}$$

The covariance matrix E_{ij} is defined as

$$E_{ij} = V_{ij} + B_{ij}. \tag{6}$$

in which i and j are the indices of the reconstructed kinetic energy bin and

$$V_{ij} = \frac{1}{N_s}\Sigma_s(\sigma_i^s - m_i)(\sigma_j^s - m_j), \tag{7}$$

$$B_{ij} = (\sigma_i^{cv} - m_i)(\sigma_j^{cv} - m_j). \tag{8}$$

V_{ij} represents the spread in bin contents around the mean of the universes and B_{ij} represents the overall bias of the mean of the universes with respect to σ^{cv}, which is the cross-section extracted in a given bin using the nominal simulation. The uncertainty in bin i is simply $\sqrt{E_{ii}}$.

For detector-related uncertainties and some cross-section model that could not be evaluated using the multisim technique, the fractional difference from the central value cross section is assigned as the systematic uncertainty. For assessing the neutrino-nucleus interaction model we vary the GENIE uncertainties based on Ref. [8]. This includes variations of the NC and CC interaction models and the Final State Interaction

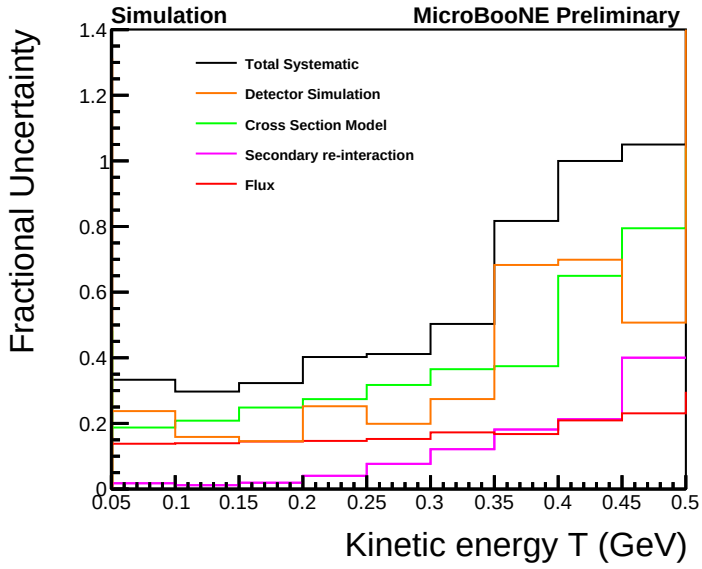

Figure 9: Summary of systematic uncertainties on the measured differential cross section. The asymmetry of the total systematic uncertainty comes from the detector-simulation component.

(FSI) model. The secondary re-interaction uncertainties come from the uncertainties of the cross section of a hadron's interaction with argon nuclei as the particles traverse the detector's medium, which could change the type and kinematics of the detected final-state particles. The uncertainties being considered include π^+, π^- and proton re-interactions, where we assume a 20% normalization uncertainty on the elastic and inelastic scattering cross sections used for secondary interactions in the GEANT4 [17] detector simulation software.

The flux uncertainty comes from the uncertainties in the production of secondary particles when the BNB protons from the primary beam collide with the beam-target, as well as the uncertainties from the magnetic horn current, the depth by which the current penetrates the conductor, and the pion and nucleon cross sections on aluminium and beryllium [18][19].

Most of the detector-simulation uncertainties are evaulated using a data-driven approach that directly modifies the simulation of the signal response as a function of the particles true kinematics and energy loss [20]. It is based on a data-driven data-MC comparison, which then is propagated to the reconstructed events by modifying the deconvolved wire waveforms. Light yield (LY) variations are another type of detector-related uncertainties which take into account the overall LY drop, the variation of Rayleigh scattering length, and light attenuation length to account for drift-distance-dependent mismodeling. In addition, uncertainty on our characterization of the electric-field non-uniformity, known as space-charge effect (SCE), the modification of the electric field due to accumulated charge from cosmic-induced slow-moving ions, is evaluated by using an alternative E-field map.

Figure 9 shows the summary of the systematic uncertainties of the differential cross section. The cross section uncertainty dominates in almost all bins. At low energy, the cross section model uncertainty mainly comes from the uncertainty on the axial form factor in the NC elastic model through the "NC Proton" background. At high energy, the large cross-section model uncertainty is caused by the large "CC Proton" background, and the low MC statistics at the high-energy bins also affect the estimation of the uncertainty. At very low energy, the detector-simulation uncertainty (mainly light yield) dominates, as our low energy signal is very sensitive to the light modeling. There appears to be a large statistical component to the detector-simulation uncertainties that could be reduced with improved MC statistics.

8 Results

Figure 10 shows the final differential cross section with all uncertainties added in quadrature, with the total uncertainty ranging from 30% to 100% at high energies. The cross section extracted from data and MC agree well in most energy bins.

It is still not clear to us what causes the data-MC difference in the lowest energy bin 0.05 to 0.1 GeV and studies are undergoing. It could be due to the x-dependent light yield modeling, as the low energy tracks are very short (about 2.3 - 7.8 cm), therefore, they are very sensitive to the light yield modeling, which is an important criteria we use to select neutrino-induced events.

In addition, the NC models used in GENIE are not well constrained by data at low energy, the data-MC difference we see in the lower energy bins could be due to physics. There are no measurements of NCE in the energy region $T < 0.225$ GeV [21]. The data-MC difference we see could be that the default axial mass and η parameters used in the NCE model [8] do not describe the shape of the cross section well at very low energy. It could also be due to the mismodeling of NC MEC interations, which has never been constrained by any data.

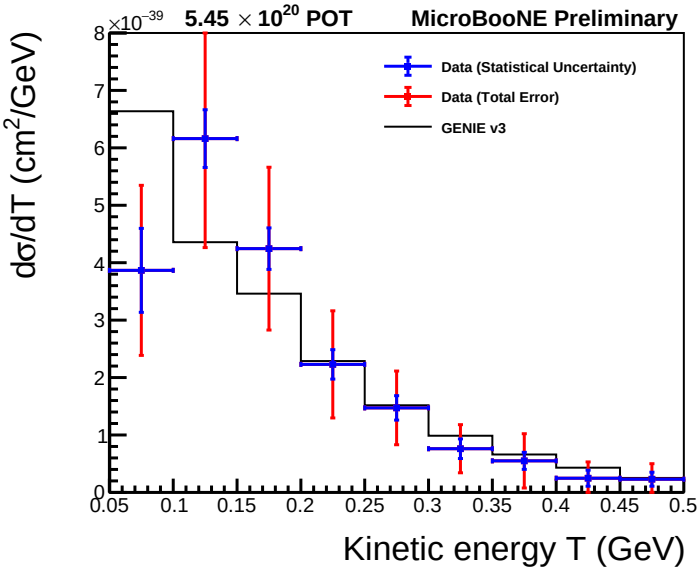

Figure 10: Final differential cross section with both statistical and systematic errors.

To summarize, we present the first NC1p inclusive differential cross section $d\sigma/dT$ on argon using 5.45×10^{20} POT beam-on data. As estimated from the MC, it includes interactions down to $Q^2 = 0.1$ GeV^2, which is significantly lower than previous measurements [21, 22].

9 Outlook

Several improvements will be carried out to improve this analysis in the near future:

1. We will further reduce the charge-current background by developing another BDT specifically targeting charge-current backgrounds, which will also reduce the cross section model uncertainty at high energy.

2. At lower energy, the dominated cross section model uncertainty comes from the "NC Proton" background events. In order to reduce the "NC Proton" background, we will perform detailed study on the candidate events that have multiple protons or both a proton and a pion in the final state. we will explore the use of side-bands to constrain the normalization uncertainties of backgrounds.

3. The current axial form factor used in GENIE relies on a dipole shape assumption that introduces an unquantified error. We will switch to "z-expansion" to describe the form factors in NC Elastic cross section, which is a model-independent, and systematically improvable, representation of axial form factor [23].

4. We will study the secondary re-interaction of neutrons, a source of uncertainty that is not considered in the current framework.

5. We expect more MC statistics would aid us in better estimating the detector-simulation systematic uncertainties.

6. We will revisit the folding method used in the cross section extraction.

7. We will compare our results with other generators (*i.e.* NuWro) to better understand the difference between data and MC model.

We also plan to report the differential cross section $d\sigma/dQ^2$. The big challenge is to understand the model-dependence of the Q^2 reconstruction, which heavily depends on the nuclear model, initial state nucleon momentum, binding energy, etc.

Our ultimate goal is to extend this measurement to a measurement of the NC Elastic cross section and the extraction of Δs.

References

[1] R. Acciarri et al. Long-Baseline Neutrino Facility (LBNF) and Deep Underground Neutrino Experiment (DUNE): Conceptual Design Report, Volume 2: The Physics Program for DUNE at LBNF. 12 2015.

[2] P. Adamson et al. Active to sterile neutrino mixing limits from neutral-current interactions in MINOS. *Phys. Rev. Lett.*, 107:011802, 2011.

[3] Katherine Woodruff. Studying Neutral Current Elastic Scattering and the Strange Axial Form Factor in MicroBooNE. *PoS*, SPIN2018:029, 2019.

[4] R. Acciarri et al. Design and Construction of the MicroBooNE Detector. *JINST*, 12(02):P02017, 2017.

[5] P. Abratenko et al. Vertex-Finding and Reconstruction of Contained Two-track Neutrino Events in the MicroBooNE Detector. 2 2020.

[6] C. Andreopoulos et al. The GENIE Neutrino Monte Carlo Generator. *Nucl. Instrum. Meth. A*, 614:87–104, 2010.

[7] Costas Andreopoulos, Christopher Barry, Steve Dytman, Hugh Gallagher, Tomasz Golan, Robert Hatcher, Gabriel Perdue, and Julia Yarba. The GENIE Neutrino Monte Carlo Generator: Physics and User Manual. 10 2015.

[8] The MicroBooNE collaboration. Neutrino Interaction Model and Uncertainties for MicroBooNE Analyses. https://microboone.fnal.gov/public-notes, MICROBOONE-NOTE-1074-PUB.

[9] C. Adams et al. Ionization electron signal processing in single phase LArTPCs. Part I. Algorithm Description and quantitative evaluation with MicroBooNE simulation. *JINST*, 13(07):P07006, 2018.

[10] C. Adams et al. Ionization electron signal processing in single phase LArTPCs. Part II. Data/simulation comparison and performance in MicroBooNE. *JINST*, 13(07):P07007, 2018.

[11] R. Acciarri et al. The Pandora multi-algorithm approach to automated pattern recognignition of cosmic-ray muon and neutrino events in the MicroBooNE detector. *J. Phys. Conf. Ser.*, 888(1):012142, 2017.

[12] https://physics.nist.gov/PhysRefData/Star/Text/PSTAR.html.

[13] The MicroBooNE collaboration. Measurement of ν_e Interactions at Low Energy with the MicroBooNE Experiment. https://microboone.fnal.gov/public-notes, MICROBOONE-NOTE-1085-PUB.

[14] The MicroBooNE collaboration. Selection of numu charged–current induced interactions with $N > 0$ protons and performance of events with $N = 2$ protons in the final state in the MicroBooNE detector from the BNB. https://microboone.fnal.gov/public-notes, MICROBOONE-NOTE-1056-PUB.

[15] A. Hoecker, P. Speckmayer, J. Stelzer, J. Therhaag, E. von Toerne, H. Voss, M. Backes, T. Carli, O. Cohen, A. Christov, D. Dannheim, K. Danielowski, S. Henrot-Versille, M. Jachowski, K. Kraszewski, A. Krasznahorkay Jr., M. Kruk, Y. Mahalalel, R. Ospanov, X. Prudent, A. Robert, D. Schouten, F. Tegenfeldt, A. Voigt, K. Voss, M. Wolter, and A. Zemla. Tmva - toolkit for multivariate data analysis, 2007.

[16] P. Abratenko et al. First Measurement of Inclusive Muon Neutrino Charged Current Differential Cross Sections on Argon at E_ν ∼0.8 GeV with the MicroBooNE Detector. *Phys. Rev. Lett.*, 123(13):131801, 2019.

[17] S. Agostinelli et al. GEANT4: A Simulation toolkit. *Nucl. Instrum. Meth. A*, 506:250–303, 2003.

[18] A. A. Aguilar-Arevalo et al. The Neutrino Flux prediction at MiniBooNE. *Phys. Rev.*, D79:072002, 2009.

[19] The MicroBooNE collaboration. Booster Neutrino Flux Prediction at MicroBooNE. https://microboone.fnal.gov/public-notes, MICROBOONE-NOTE-1031-PUB.

[20] The MicroBooNE collaboration. Novel Approach for Evaluating Detector Systematics in the MicroBooNE LArTPC. https://microboone.fnal.gov/public-notes, MICROBOONE-NOTE-1075-PUB.

[21] L.A. Ahrens et al. Measurement of Neutrino - Proton and anti-neutrino - Proton Elastic Scattering. *Phys. Rev. D*, 35:785, 1987.

[22] A.A. Aguilar-Arevalo et al. Measurement of the Neutrino Neutral-Current Elastic Differential Cross Section on Mineral Oil at $E_\nu \sim 1$ GeV. *Phys. Rev. D*, 82:092005, 2010.

[23] Aaron S. Meyer, Minerba Betancourt, Richard Gran, and Richard J. Hill. Deuterium target data for precision neutrino-nucleus cross sections. *Phys. Rev. D*, 93(11):113015, 2016.